JOURNAL OF GEOPHYSICAL RESEARCH, VOL. 113, D16102, doi:10.1029/2007JD009555, 2008

Seasonal and interannual variations of Amur River discharge and their relationships to large-scale atmospheric patterns and moisture fluxes

Yoshihiro Tachibana,[1,2] Kazuhiro Oshima,[3] and Masayo Ogi[4,5]

Received 31 October 2007; revised 24 April 2008; accepted 6 May 2008; published 16 August 2008.

[1] Using reanalysis data, we investigate the relationship of Amur River discharge and vertically integrated atmospheric horizontal moisture flux. The discharge has two peaks, one in May (spring) and the other in September (autumn). Comparison of the moisture flux convergence to the discharge indicates that the spring peak is supplied by the flux in previous seasons (September through April), whereas the autumn peak is supplied by the summertime flux (May through August). A northward flux associated with storm activities in the previous autumn and winter contributes to the spring discharge. The autumn discharge is mainly supplied by a northward flux associated with the Asian summer monsoon and by an eastward flux originating from evaporation in the far western inland part of Eurasia. Interannual variation in the flux and discharge is also investigated. The strong Asian summer monsoon associated with anomalous cyclonic circulation over Eurasia strengthens the summer flux convergence at an interannual time scale, resulting in anomalously large discharge in autumn. The strong Asian winter monsoon wind with a dry air mass, associated with the anomalously strong Siberian high and Aleutian low, activates evaporation. This results in anomalously large flux divergence in autumn through winter and anomalously small discharge in spring. The anomalously large spring discharge is related to the warm phase of the Arctic Oscillation. This suggests that the rapid melting of snow and frozen soil contributes to the spring discharge. These results indicate that the Asian monsoon plays an important role in the freshening of the Okhotsk Sea, in which sea ice forms with extremely low salinity.

Citation: Tachibana, Y., K. Oshima, and M. Ogi (2008), Seasonal and interannual variations of Amur River discharge and their relationships to large-scale atmospheric patterns and moisture fluxes, *J. Geophys. Res.*, *113*, D16102, doi:10.1029/2007JD009555.

1. Introduction

[2] The Amur River, with a basin area of 1.86×10^6 km^2, is the fourth largest river in northern Eurasia and supplies much of the fresh water to the Okhotsk Sea, one of the southernmost ice-covered seas in the Northern Hemisphere (Figure 1). Freshwater discharge from the Amur River, which causes large stratification that suppresses deep convection and promotes freezing, is an important factor controlling the formation of sea ice [e.g., *Akagawa*, 1977]. This situation is quite similar to that of other large rivers discharging into the Arctic Ocean [e.g., *Alekseev et al.*, 2000]. Sea ice formation in the Okhotsk Sea plays an important role in the formation of the North Pacific intermediate water [e.g., *Yasuda*, 1997]. Greater knowledge of the atmospheric conditions that determine Amur River discharge is important for understanding the freshwater budget in the Okhotsk Sea. Although many studies have examined at the discharge of other rivers in northern Eurasia in association with large-scale atmospheric circulations [e.g., *Fukutomi et al.*, 2003; *Serreze et al.*, 2002; *Su et al.*, 2006], relatively few have focused on the Amur River. Knowledge of the basic hydroclimatological characteristics of the Amur River is also lacking. According to *Ogi et al.* [2001], the climatological annual amount of discharge from the Amur River is 333 km^3/a (10,929 m^3/s). A distinctive characteristic of the annual cycle of the Amur River is its two discharge peaks, one in June and the other in September. The Amur River is the only river in northern Eurasia to have double peaks (K. Masuda, personal communication, 2007). *Ogi et al.* [2001] speculated that the first peak occurs because of melting snowpack and frozen soil, whereas the second peak is caused by summertime monsoon precipitation. The snowpack likely accumulates from snowfall during the previous autumn through winter.

[3] In addition, few papers have described the interannual variability of the Amur River. *Ogi and Tachibana* [2006]

[1]Institute of Observational Research for Global Change, Japan Agency for Marine-Earth Science and Technology, Yokosuka, Japan.
[2]Also at Faculty of Bioresources, Mie University, Tsu, Japan.
[3]Faculty of Environmental Earth Science, Hokkaido University, Sapporo, Japan.
[4]Joint Institute for the Study of the Atmosphere and Ocean, University of Washington, Seattle, Washington, USA.
[5]Also at Frontier Research Center for Global Change, Japan Agency for Marine-Earth Science and Technology, Yokohama, Japan.

0148-0227/08/2007JD009555$09.00

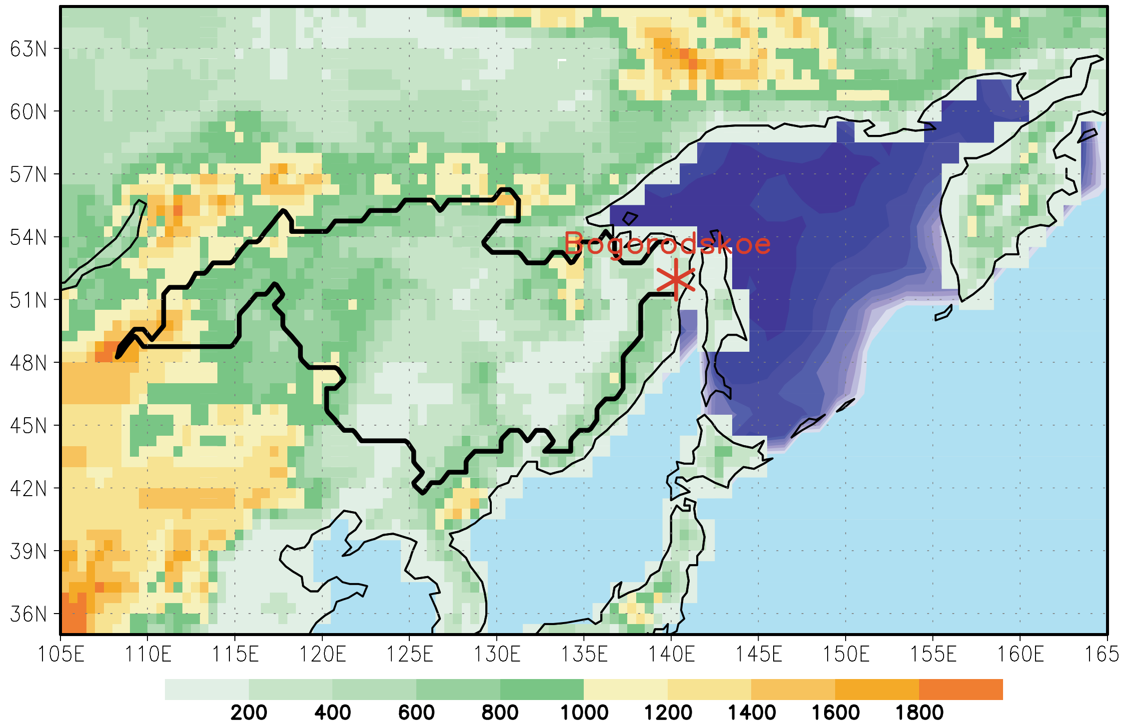

Figure 1. Map of the Amur basin. The black lines drawn on the continent show the drainage boundaries obtained from the TRIP river basin data set [*Oki and Sud*, 1998]. The asterisk indicates the location of the Bogorodskoe observation station, the station at the lowest reaches of the Amur River among all runoff observation stations in the basin. The gradation of green and brown shadings shows the altitude at 200-m increments. The dark blue color with contours on the Okhotsk Sea indicates the sea ice concentration in March 2001 from the Hadley Ice and Sea Surface Temperature (HadISST) data set. The contour interval of the sea ice is from 10% to 100%.

found that the interannual variation in Amur discharge is related to the annual mean Northern Hemisphere Annular Mode/Arctic Oscillation (NAM/AO). The positive NAM/AO is characterized by an anomalous low surface pressure field in the Arctic and an anomalous high surface pressure field in the midlatitudes [*Thompson and Wallace*, 1998]. In years of positive NAM/AO, annual mean Amur discharge is larger than normal. Because there are two peaks in the discharge, the large-scale atmospheric patterns and local-scale storm tracks governing the spring discharge peak must differ from those governing the autumn peak. However, no previous studies have clarified the large-scale atmospheric patterns and local-scale storm tracks that determine individual discharge peaks. Basic knowledge of the hydrometeorology of the Amur River remains insufficient.

[4] Past studies have commonly applied vertically integrated atmospheric horizontal moisture flux analysis, using reanalysis and river discharge data, to rivers flowing toward the Arctic [e.g., *Fukutomi et al.*, 2003; *Serreze et al.*, 2002]. This method might indicate the origins of the moisture that becomes river runoff. The moisture flux pattern in association with river discharge also indicates the large-scale atmospheric pattern governing discharge. For the long-term mean, mass conservation law requires that the convergence of the atmospheric moisture flux over a river basin equals the amount of river runoff [e.g., *Oki et al.*, 1995; *Masuda et al.*, 2001]. However, the convergence calculated using one reanalysis data set often differs from that calculated using another reanalysis data set because of different data assimilation methods. The comparison of moisture flux convergence with river runoff provides a diagnosis of a reanalysis data set if true runoff is known [*Masuda et al.*, 2001]. *Inoue and Matsumoto* [2004] found that two reanalysis data sets showed different sea level pressure (SLP) fields over north Asia. Because this area is near the Amur basin, the diagnosis of many reanalysis data sets over the Amur basin by comparison with river runoff can provide important information.

[5] *Hirschi et al.* [2006] applied moisture flux convergence analysis to approximately 30 large rivers, but only briefly described the Amur River. Further, although they speculated that Amur River discharge might be related to the Asian monsoon, they did not provide any evidence. Their speculation suggests that a source region of the moisture is the Pacific. Another possible moisture source is an inland area of the Eurasian continent. According to a tagged water experiment using an atmospheric general circulation model simulation by *Numaguti* [1999], the summer precipitation in northern Eurasia partially originates from water vapor that evaporates from inland areas of the Eurasian continent. However, because of the lack of detailed study of the moisture flux associated with the Amur River, the moisture source remains unclear.

[6] Our analysis has two aims. One is to diagnose the reanalysis data sets produced by the following organizations: the European Centre for Medium-Range Weather Forecasts (ECMWF), the National Centers for Environmental Prediction (NCEP), and the Japan Meteorological Agency (JMA). By comparison with observed river discharge data, we will deter-

mine which reanalysis data set is closest to the observed discharge in this region. Our other aim is to determine which atmospheric patterns govern the spring and autumn discharge peaks. Using the most accurate reanalysis data set, we will illustrate the origin of the moisture. Moreover, we will determine the interannual variations in the atmospheric patterns that influence the two discharge peaks. Our results will provide a basic understanding of the effects of atmospheric forcing on Amur River discharge, which influences the physical, chemical, and biological environments of the Okhotsk Sea.

2. Data

[7] Monthly mean Amur River discharge data from 1980 through 2001 are used for the analysis. These data were recorded at Bogorodskoe, the lowest-reach hydrological station of the Amur River at which discharge has been routinely measured by the Far Eastern branch of the Russian Federal Service for Hydrometeorology and Environmental Monitoring (FERFSHEM). According to FERFSHEM, river discharge is measured at least twice per month. Current speeds are measured from an observation ship at approximately 10 points across the river at two depths. The river width along the baseline is approximately 2–3 km, depending on the water level. FERFSHEM also measures the water level daily. When a large increase in water level occurs, current speed is also measured. The lower stream of the Amur basin is covered by huge bogs and swamps, with numerous meandering branches of the river. Floods sometimes turn these bogs and swamps into large ponds. The Bogorodskoe observatory is located in a small canyon in which there are no river branches in any season and no influence of ocean tides. In winter, current speed is measured at the observatory through holes cut through the frozen river. These observation conditions suggest that the accuracy of the observed discharge is quite high. We also use monthly mean river water temperature measured at Bogorodskoe from 1987 through 2001.

[8] Four sets of atmospheric reanalysis data are used: ECMWF 40-year reanalysis (ERA40) [*Uppala et al.*, 2005], ECMWF 15-year reanalysis (ERA15) [*Gibson et al.*, 1997], NCEP reanalysis 2 (NCEP2) [*Kanamitsu et al.*, 2002], and JMA 25-year reanalysis (JRA25) [*Onogi et al.*, 2007]. The time resolution of these data is 6 hourly, except for the ERA15 data, which have 12 hourly resolution. The horizontal resolution of the former three reanalysis sets is $2.5° \times 2.5°$ and that of JRA25 is $1.25° \times 1.25°$. The analysis period is from 1979 through 2001, except for ERA15, which is from 1979 through 1993. Reanalysis data before 1979 were excluded because of possible shortcomings in data obtained during the presatellite era.

[9] Moreover, we use precipitation and snow cover data over the Amur basin as supplementary data to exhibit environmental hydroclimatological features. The precipitation data are from the recently opened data set Asian Precipitation-Highly Resolved Observational Data Integration toward Evaluation of the Water Resources (APHRODITE's Water Resources) [*Xie et al.*, 2007] and have a spatial resolution of $0.5° \times 0.5°$. The snow cover data are NOAA/National Environmental Satellite, Data, and Information Service (NESDIS) and Climate Prediction Center (CPC) NH snow cover data with $2° \times 2°$ spatial resolution [*Robinson et al.*, 1993]. The analysis periods for precipitation and snow cover are 1980–2000 and 1980–1999, respectively.

3. Methods

[10] We used horizontal moisture flux analysis to calculate the net precipitation (precipitation minus evaporation; hereafter P-E) in the Amur basin. We further separate the moisture flux into two time scales: moisture flux transported by atmospheric large-scale stationary waves, which are related to planetary waves, and moisture flux transported by short-time-scale transient eddies, which are mainly related to storm tracks. The separation of these scales allows the determination of what types of atmospheric pattern are mainly associated with the discharge.

[11] *Oki et al.* [1995] provided detailed formulations for calculating the connectivity of the horizontal moisture flux with river discharges. Here, we briefly summarize these formulations and add an explanation of the method for dividing the stationary and transient components of the flux. P-E is estimated using the atmospheric moisture budget equation as follows:

$$\frac{\partial PW}{\partial t} = -\nabla < q\mathbf{v} > +E - P, \tag{1}$$

where PW is precipitable water, q is the specific humidity, and $\boldsymbol{v}$ is the wind vector. The angled brackets indicate vertical integration from the surface to the 300-hPa level. Therefore, $<q\boldsymbol{v}>$ represents the vertical integral of horizontal moisture flux. We defined the Amur basin region from the Total Runoff Integrating Pathways (TRIP) river basin data set [*Oki and Sud*, 1998]. On the basis of the TRIP data set, P-E is estimated from the area-weighted average values of PW and the horizontal convergence of $<q\boldsymbol{v}>$ over the area of the Amur basin (Figure 1).

[12] Water vapor in the midlatitudes is transported by both atmospheric stationary waves and moving transient eddies. Because the temporal scales of these two transports are quite different, dividing the moisture flux into these two categories provides useful information on the atmospheric causes of the discharge [*Oshima and Yamazaki*, 2004, 2006]. In accordance with the method formulated by *Oshima and Yamazaki* [2004, 2006], we divide the monthly mean total moisture flux into stationary flux and transient flux as follows:

$$< \overline{q\mathbf{v}} > = < \overline{q}\ \overline{\mathbf{v}} > + < \overline{q'\mathbf{v}'} >, \tag{2}$$

where the overbars represent a time average calculated using the monthly average, and the primes represent the deviation from the monthly average. The stationary flux is calculated from the monthly mean fields of wind, moisture, and surface pressure. The transient flux is obtained by subtracting the stationary flux from the total flux.

[13] Next, the connectivity of the horizontal moisture flux and the river discharge is described. Using the terrestrial water budget equation, the time rate of change in land water storage, S, is written as

$$\frac{\partial S}{\partial t} = P - E - R, \tag{3}$$

Table 1. Comparison of the Climatological P-E Estimated by ERA40, NCEP2, JRA25, and ERA15 Reanalysis Data and the Observed Amur River Discharge Data[a]

	ERA40	NCEP2	JRA25	ERA15	Amur
Annual P-E	182	178	116	(69)	190 (202)
Summer P-E	113	124	48	(57)	121 (128)
Winter P-E	69	54	68	(15)	69 (69)

[a]The unit is mm/a. The values in the "Amur" column are the amount of discharge divided by the area of the Amur basin. The summer value for the Amur column is the autumn discharge corresponding to the summer P-E, and the winter value for the Amur column is the spring discharge corresponding to the winter P-E. Figure 2 shows the months of each period. The calculation period for the reanalysis data is 1979 through 2001, except for ERA15, which is from 1979 through 1993. The Amur values correspond to climatological mean discharge. Brackets indicate the average P-E and discharge between 1979 and 1993.

where R is the river runoff. The resulting output, R, is then written as

$$R = -\frac{\partial S}{\partial t} - \nabla < q\mathbf{v} > -\frac{\partial PW}{\partial t} = -\frac{\partial S}{\partial t} + P - E. \qquad (4)$$

Equation (4) indicates that R is determined by $\partial S/\partial t$ and P-E. Because the term $\partial S/\partial t$ acts as resistance or capacitance, the R response usually lags behind the P-E input. If we calculate an average over a long time period (e.g., multiyear mean), $\partial S/\partial t$ in equation (3) is negligible. By averaging over the river basin area, the river discharge is thus equal to the estimated P-E. The comparison of the climatological mean annual P-E to the climatological mean annual discharge provides the degree of accuracy of the moisture flux in the reanalysis data sets.

4. Comparison of Discharge to Net Precipitation Estimated by Reanalysis Data

[14] Table 1 provides the climatological P-E estimated by comparison of the four reanalysis data sets with observational discharge data (the discharge is divided by the area of the Amur basin). The annual mean discharge of the Amur River is 190 mm/a. The annual mean P-E from the ERA40 (182 mm/a) is closer to the observed annual discharge compared to that from the other reanalysis data; however, even the ERA40 data underestimate the annual mean P-E. The ERA15 (69 mm/a) shows poor accuracy. The JAR25 (116 mm/a) is better than the ERA15, but worse than the ERA40 and NCEP2 (178 mm/a). The seasonal means values have the same tendency as the annual mean values. The underestimation resulting from the JRA25 is caused by the small values for humidity and wind convergence in the lower troposphere in summer compared to the other reanalysis data (H. Hatsushika, chief member of the JRA25 reanalysis project, personal communication, 2007). *Masuda et al.* [2001] reported that the sign of the flux convergence of the NCEP reanalysis 1 is negative (i.e., P-E is negative) for some large rivers in other regions of the world, implying no river runoff. Considering the poor results for other areas, we can regard the overall accuracy of all of the reanalysis data sets as good for the Amur region. In our study, although P-E over the Amur River basin is underestimated by the ERA15 and JRA25, it is still positive. As described further in section 7, the interannual variation estimated by P-E from the ERA40 data is closest to the observed discharge. Therefore, we hereafter show the results calculated using the ERA40 data.

5. Annual Hydroclimatological Cycle

[15] Figure 2a shows the annual hydroclimatological cycles of the Amur River. The river has two discharge peaks: in May and September. A single peak in P-E occurs in July; approximately 2 months later, another discharge peak occurs in autumn, reflecting the influence of land surface processes, S; these processes strongly depend on the season. The value of $\partial S/\partial t$ in Figure 2a is calculated from equation (3). It is notable that the minimal discharge occurs in July, the month in which water supply by P-E is maximal. Figure 2b shows other climatological conditions over the Amur basin. The temperature at 2 m height changes from negative to positive in April and back to negative in October. This indicates that precipitation accumulates as snow from October to March and that the accumulated snow and frozen soil start to melt in April. Satellite observations indicate maximum snow coverage in January, a large decline beginning in April, and accumulation starting again in October. This suggests that snowmelt starts in April and that the discharge peaks in May with the decrease in storage. The seasonal cycle of river water temperature has an annual cycle similar to that of temperature at 2 m. The river water temperature becomes positive in May, indicating that frozen river water begins to melt in this month. In summer, the river water temperature is approximately 20°C. This implies that warm river water is supplied to the cold Okhotsk Sea, of which the sea surface temperature in summer is approximately 10°C [*Ogi et al.*, 2001]. The river water temperature falls to zero in November, and the river starts to freeze. Precipitation estimated using APHRODITE data peaks in July at approximately 1400 mm/a and has a minimum in February. The annual cycle of precipitation has a pattern quite similar to that of P-E. Thus, the P-E peak in July is mainly related to the precipitation in summer. PW is also maximal in July and minimal in January. The evaporation, which can be roughly estimated by subtracting P-E from the precipitation, is approximately more than half of the precipitation in most months.

[16] The blue and black lines in Figure 3 show the mean annual climatological cycle of the moisture flux convergence and the P-E averaged over the Amur basin, respectively. The annual P-E cycle is similar to that of the moisture flux convergence, except in spring and autumn. These differences reflect the large changes in PW in spring and autumn (Figure 2b). The red and green lines in Figure 3 show the annual climatological cycle of the stationary and the transient components of the horizontal moisture flux convergence, respectively. In summer, moisture is mainly transported by stationary waves, whereas in autumn and winter, moisture is transported by both transient eddies and stationary waves.

6. Spring and Autumn Discharge and Their Relationship to Net Precipitation

6.1. Periods of Spring and Autumn Discharge and Associated Periods of Winter and Summer P-E

[17] The seasonal variation in discharge is not equal to that in net precipitation (P-E) because of the large value of $\partial S/\partial t$ at this time scale. Also, S strongly depends on the

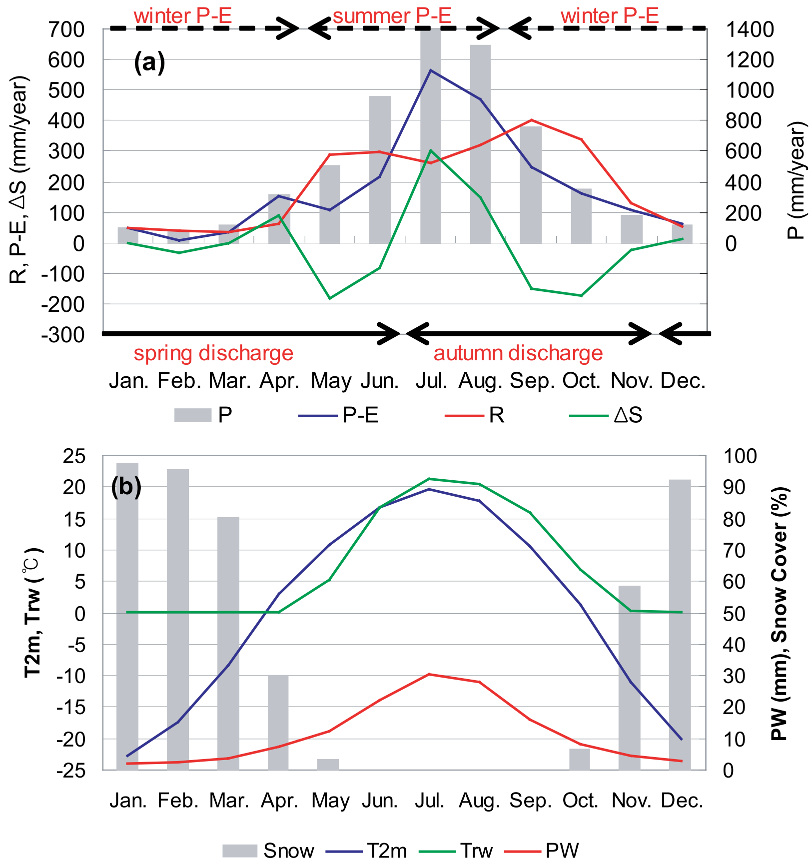

Figure 2. (a) Climatology of the month-to-month variation in Amur River discharge (red line), net precipitation (precipitation minus evaporation, P-E) calculated by the ERA40 over the Amur basin (blue line), and the change in land water storage, $\partial S/\partial t$ (green line). The unit for these lines is mm/a. The discharge is divided by the area of the Amur basin. Bar graphs show the climatology of month-to-month variation in area-weighted average precipitation over the Amur basin estimated by APHRODITE data. The unit is mm/a. Two arrows drawn along the horizontal axis indicate the periods defined as the spring and autumn discharge periods. The two arrows with dashed lines at the top indicate the periods of P-E that supplied the spring and autumn discharge. (b) Climatology of the month-to-month variation in precipitable water over the Amur basin calculated by the ERA40 (red line), area-weighted average temperature at 2 m height over the Amur basin calculated by the ERA40 (blue line), and river water temperature at Bogorodskoe (green line). Bar graphs indicate snow coverage over the Amur basin estimated by NOAA/NESDIS data. The units for temperature, precipitable water, and snow coverage are °C, mm, and %, respectively.

season. From autumn through winter, precipitation accumulates as snow, whereas in summer, the precipitation is expected to discharge within a short time. The time lag of the autumn discharge peak behind the P-E peak is related to the fact that runoff takes approximately 2 months to reach the outlet of the basin, given the massive size of the Amur basin. We first confirm the months of P-E that cause the respective climatological spring and autumn discharge.

[18] On the basis of the two clear discharge peaks shown in Figure 2b, we define December through June as the months of spring discharge and July through November as the months of autumn discharge. The climatological spring discharge is 121 mm/a and the autumn discharge is 69 mm/a. We want to determine the periods of summer and winter P-E that correspond to the spring and autumn discharge, respectively. A pair of time-averaged P-E as a function of the beginning and ending months is calculated to compare the spring and autumn discharge. For example, one pair consists of the average from May through August (denoted as $PE1_i$) and the average for the rest of the months, i.e., the average from September through April (denoted as $PE2_i$). Another pair, for example, consists of the average from May through September ($PE1_{i+1}$) and that for the rest of the months, i.e., the average from October through April ($PE2_{i+1}$). The number of all probable pairs is mathematically equal to a permutation, ${}_{12}P_2$, i.e., 132. The time-averaged P-E in each period changes with the chosen months (i = 132). The root mean square error (RMSE), i.e., $(PE1_i - 121\ \mathrm{mm/a})^2 + (PE2_i - 69\ \mathrm{mm/a})^2$ is calculated for all of the 132 pairs. We then search for the pair with the smallest RMSE and reject hydrologically unlikely sets. The pair identified using this procedure is regarded as showing the periods of the spring and autumn discharge.

[19] On the basis of this procedure, the time averaged P-E from May through August corresponds to the autumn discharge, and that from September through April corre-

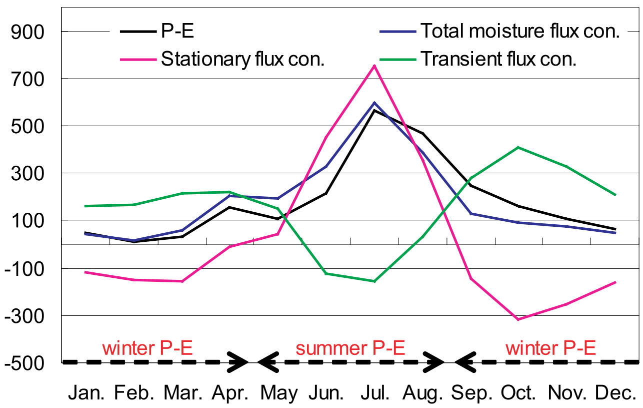

Figure 3. Climatology of month-to-month variation in the horizontal convergence of the moisture flux and the P-E over the Amur basin calculated by ERA40 data. The stationary and transient components of the flux convergence are also drawn. The stationary component is calculated by the monthly mean atmospheric fields, and the transient component is calculated by the total flux minus the stationary component. The unit is mm/a.

sponds to the spring discharge. Hereafter, we refer to May through August as the summer moisture flux or the summer P-E, and September through April as the winter moisture flux or the winter P-E. The defined periods and their corresponding seasons of P-E are schematized using arrows in Figure 2a. The autumn discharge lags behind the summer P-E by approximately 2 months. In contrast, the period of winter P-E that brings the spring discharge is longer than the period that brings the autumn discharge. The amounts of summer P-E and winter P-E closely agree with those of spring and autumn discharge, respectively (Table 1).

6.2. Climatological Moisture Flux Patterns in Summer and Winter

[20] As indicated in Figure 3, the main component of the moisture flux related to the autumn discharge is different from that related to the spring discharge. In the summer flux period, the stationary component is dominant, whereas for the winter flux period, the transient component plays a principal role in supplying the water vapor in the Amur basin. The stationary component in the winter flux period is negative. These differences imply that different atmospheric circulation patterns are related to the discharge in the respective periods.

[21] Figure 4 shows climatological moisture flux fields for the stationary and transient components and their totals in winter (September to April) and summer (May to August). In summer, the stationary component, in which arrows overall point northeastward over the Amur basin, mainly determines the total flux convergence. An area with long arrows from the East China Sea to Japan marks the rain belt that coincides with the Baiu/Meiyu stationary front, in association with the Asian summer monsoon [e.g., *Yoshino*, 1965; *Murakami and Matsumoto*, 1994]. This area also covers the southeastern part of the Amur basin. Therefore, the summer flux, which influences the autumn discharge, is partially influenced by the Asian summer monsoon. Flux from the west of the Amur basin also contributes to the summer precipitation. This eastward flux can be caused by midlatitude westerlies. Divergent areas are located in the far western inland area of the continent. Because the divergent sign of the vertically integrated horizontal flux must equal the moisture supply from the surface, the divergent area indicates that surface evaporation exceeds precipitation there. Therefore, Figure 4 implies that water vapor that evaporates from inland areas also supplies precipitation to the Amur basin. This is consistent with the results of a tagged water experiment with an atmospheric general circulation model by *Numaguti* [1999], who suggested that precipitation in northern Eurasia originates from water vapor that evaporates from inland areas of the Eurasian continent and that this evaporation-precipitation process is repeated several times within the continent, in effect recycling the water.

[22] The transient component of the flux diverges overall over the Amur basin in summer. This implies that short-lived cyclones, in association with a midlatitude baroclinic zone, do not supply water to the Amur basin in summer. Northward directed arrows indicate that the moisture that evaporates in the Amur basin is transported further north in association with short-lived summertime cyclones and anti-cyclones.

[23] In winter, the overall flux by the transient component converges over the Amur basin, whereas the flux by the stationary component diverges overall. The flux convergence of the transient component can be caused by storm activity in this season and region, where wintertime cyclones are known to begin and develop [e.g., *Chen et al.*, 1991]. Arrows in the transient component suggest that the river water in the spring discharge originates from the Pacific, although these arrows are not the same as the material trajectories. In contrast, arrows in the stationary component around the Amur basin point southeastward. This direction is associated with the winter monsoon that blows from the cold, dry Eurasian continent toward the warm Pacific Ocean. Evaporation due to the stationary component associated with the dry monsoon wind over the Amur basin can cause the divergence of the horizontal moisture flux (i.e., negative water input to the Amur basin). Overall, the total flux in winter slightly converges over the Amur basin because of larger moisture flux from the south by the transient component than by the stationary component.

[24] In summary, the spring discharge is mainly supplied by water vapor from the Pacific Ocean transported by short-lived storm activity in winter. The autumn discharge is mainly supplied by water vapor from the East China Sea in

Figure 4. Climatological horizontal maps of (left) summer (May through August) and (right) winter (September through April) moisture fluxes and their divergence or convergence calculated by ERA40 data. (top) Total, (middle) stationary, and (bottom) transient components. Arrows represent the flux, with the unit length shown in each map. The unit of flux is kg s^{-1} m^{-1}. The shading indicates the divergence or convergence in mm/d. The turquoise and reddish colors represent convergence and divergence, respectively. The length of the arrows for the transient component is three times as long as the arrow in the total or stationary flux figures when the flux value is of identical magnitude.

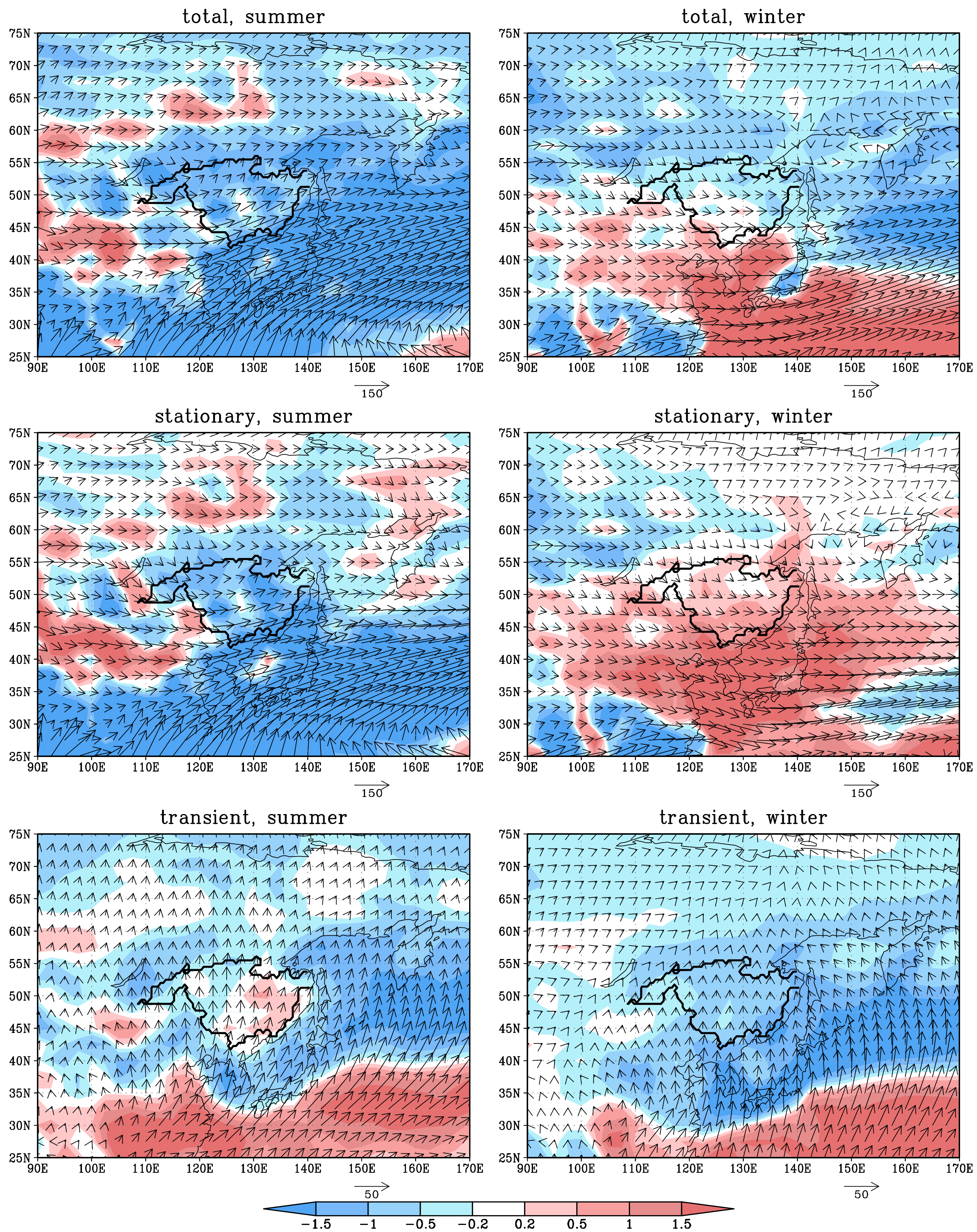
total, summer
total, winter
stationary, summer
stationary, winter
transient, summer
transient, winter
75N
70N
65N
60N
55N
50N
45N
40N
35N
30N
25N
90E
100E
110E
120E
130E
140E
150E
160E
170E
150
50
−1.5
−1
−0.5
−0.2
0.2
0.5
1
1.5

Figure 4

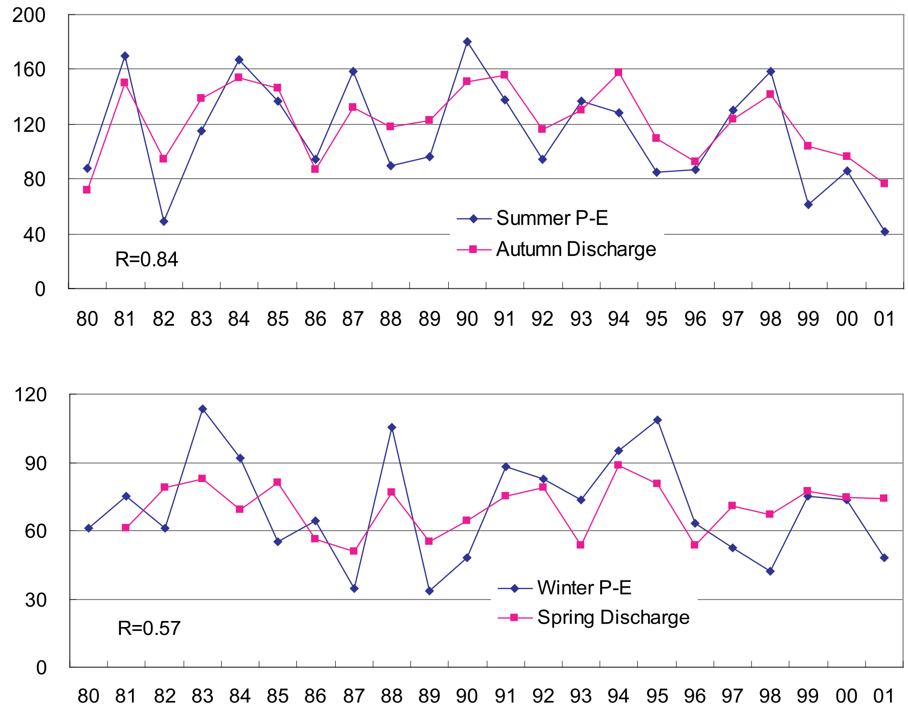

Figure 5. (top) Interannual variation in autumn discharge and the corresponding summer P-E calculated by ERA40 data and (bottom) that in spring discharge and its corresponding winter P-E. The year "01" on the *x* axis of Figure 5 (bottom) indicates the mean value from September to December of the year 2000 plus the value from January to April of 2001 for the winter P-E, and from December 2000 plus January to June 2001 for the spring discharge. The unit of the vertical axis is mm/a. The discharge is divided by the area of the Amur basin. The "R" shown in each plot indicates the correlation coefficient between P-E and discharge.

association with the Asian summer monsoon, as well as evaporated water from inland areas carried by midlatitude westerlies.

7. Interannual Variation and Its Relationship to Horizontal Moisture Flux Patterns

[25] Next, we investigate the causes of interannual variation in Amur River discharge. Because different climatological atmospheric processes cause the spring and autumn discharges, analyses of the interannual variation must also be divided into these two seasons. Figure 5 shows time series of spring and autumn discharge and their associated winter and summer P-E. Correlation coefficients are 0.84 for autumn discharge and summer P-E and 0.57 for spring discharge and winter P-E. Autumn discharge thus shows better correlation than spring discharge. The large correlation for autumn discharge indicates that summer atmospheric processes principally govern autumn discharge. On the other hand, spring discharge is influenced not only by atmospheric processes related to the P-E, but also by other major hydrological processes that are affected by variation in water storage, *S*. Calculating the interannual variations from the NCEP-R2 and JRA25 data and correlating these variations with the discharge (Table 2) again confirms the superiority of the ERA40 data.

[26] Table 3 provides the correlation coefficients of the interannual time series of the individual stationary and transient components of the flux convergence with the time series of the total moisture flux convergence. The variations in the total moisture flux convergence correlate well with the stationary components in both seasons. The higher correlations with the stationary components than with the transient components indicate that the variances of the stationary components in both summer and winter are much

Table 2. Correlation Coefficients of Autumn Discharge and the Corresponding Summer P-E Estimated by ERA40, NCEP2, JRA25, and ERA15 Reanalysis Data on an Interannual Time Scale and Those of Spring Discharge With the Corresponding Winter P-E[a]

	ERA40	NCEP2	JRA25	ERA15
Autumn discharge	0.84**	0.74**	0.74**	0.77**
Spring discharge	0.57**	0.54*	0.51*	0.23

[a]Double and single asterisks denote 99% and 95% statistical significance (*t* test), respectively.

Table 3. Correlation Coefficients for the Stationary, Transient, and Total Moisture Flux Convergences Averaged Over the Amur Basin Calculated by ERA40 Data on an Interannual Time Scale[a]

Season	Total and Stationary	Total and Transient	Stationary and Transient
Summer	0.80**	0.29	−0.34
Winter	0.70**	0.24	−0.53*

[a]For example, "total and stationary" indicates the correlation coefficient between the total and stationary flux convergences. Double and single asterisks denote 99% and 95% statistical significance (*t* test), respectively.

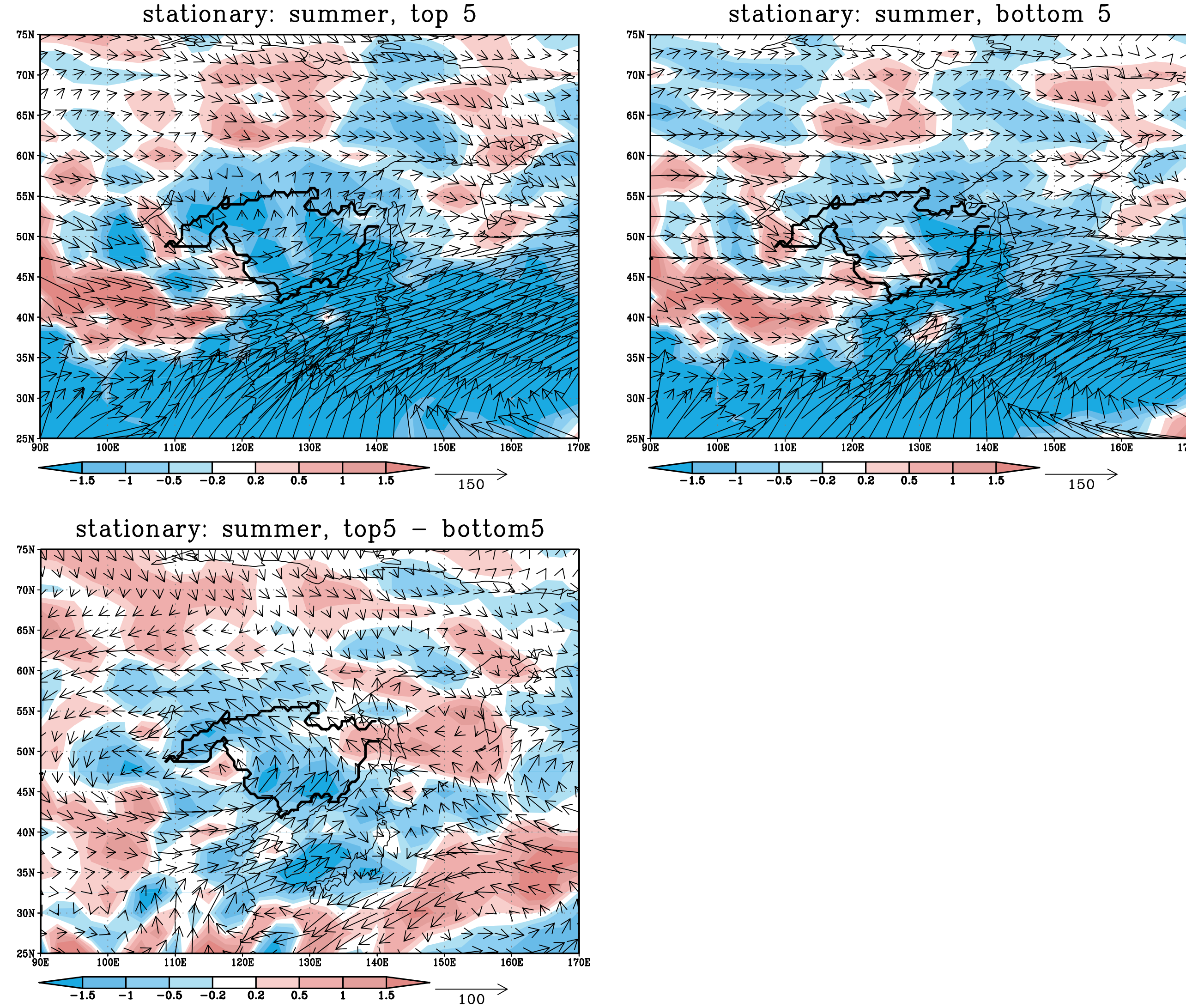

Figure 6. As in Figure 4 except for the composite maps of the summer moisture flux of the stationary component and their divergence or convergence in (top left) the top five summer P-E years and (top right) the bottom five summer P-E years. (bottom) A deviation map of the top 5 years from the bottom 5 years. The arrows in the deviation map are 1.5 times as long as the arrows in the maps of the top and bottom 5 years when the flux value is of identical magnitude.

larger than those of the transient components. Therefore, the stationary components are the prime determinant for the interannual variation in discharge. There are negative correlations between the stationary and transient components, particularly in winter. These negative correlations suggest the presence of the connection of an atmospheric planetary wave pattern with the transient storm track activity at an interannual time scale. This interesting issue is beyond the scope of our analysis.

[27] Now, we examine moisture flux patterns in association with the interannual variation in spring and autumn discharge. Figure 6 shows the composite maps of the moisture fluxes in years of large (top 5) and small (bottom 5) summer P-E. Moisture flux fields in years of large summer P-E over the Amur basin show counterclockwise circulation centered in the west of the basin for the stationary component. For this flux pattern, the moisture tends to come from the Pacific to the southeastern Amur basin. In contrast, the years of small summer P-E exhibit no prominent counterclockwise circulation pattern. The flux in the years of small summer P-E is more zonal than in the years of large summer P-E. The source region of the water in the years of small summer P-E is thus mainly in inland continental areas. Figure 6 also shows the flux difference between years of large and small summer P-E. A counterclockwise anomalous moisture flux pattern is obvious over the continent, suggesting that anomalous moisture flux from Southeast Asia also promotes anomalous P-E in the Amur basin, which then leads to anomalous autumn discharge.

[28] The flux difference appears smaller in winter than in summer. As shown in Figure 7, the patterns for years of both large and small winter P-E are similar to those of the climatology (Figure 4). The differences in the flux fields between years of large and small winter P-E exhibit a

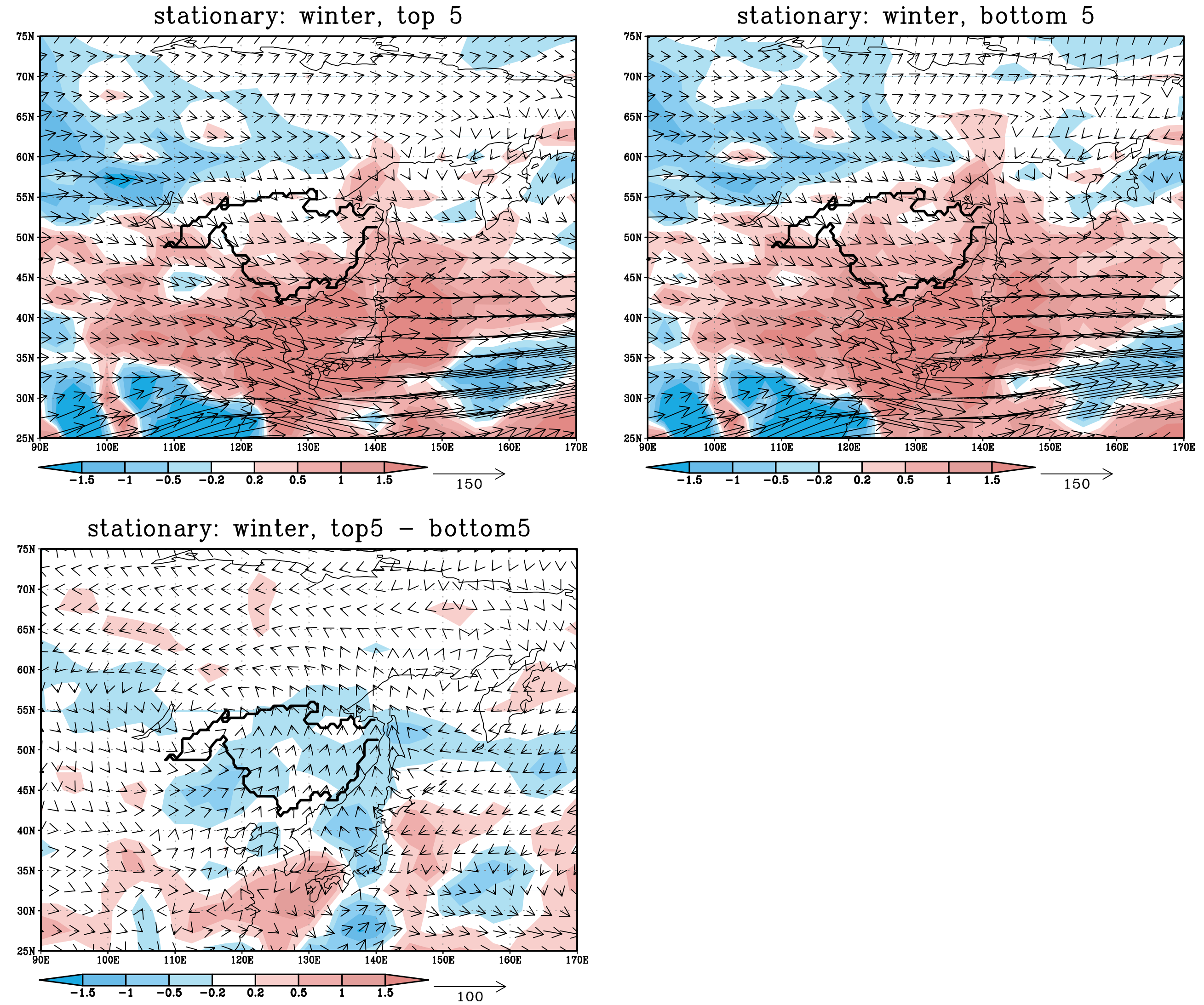

Figure 7. As in Figure 6 except for winter.

counterclockwise circulation pattern centered on the west of the Amur basin. The counterclockwise pattern and the overall northward orientation in the Amur basin suggest the weakness of the Asian winter monsoon.

8. Interannual Variation and Its Relationship to Large-Scale Atmospheric Patterns

[29] Large-scale atmospheric fields linearly regressed onto the interannual variation in the stationary component of the moisture flux convergence are shown in Figures 8 and 9. The time series of the stationary component is normalized by its standard deviation. A notable feature in the circum-Amur basin area in summer is the presence of negative anomalies over the eastern Eurasian continent centered near Lake Baikal in the sea level pressure (SLP), 500-hPa, and 200-hPa height fields, signifying a barotropic structure. Cold anomalies can be also seen around Lake Baikal (Figure 8b). The location of the cyclonic circulation anomaly in association with the cold anomalies is located just to the west of the Amur basin. This cyclonic circulation agrees with the counterclockwise moisture flux pattern of the stationary component in the years of large summer P-E (Figure 6). Also, positive anomalies over the Okhotsk Sea can be seen in the SLP field. The signature of the positive anomalies over the Okhotsk Sea is related to the appearance of the Okhotsk high, which occasionally appears over the Okhotsk Sea in summer [*Tachibana et al.*, 2004]. The contrast between the anomalous low pressure over land and the anomalous high pressure over the Okhotsk Sea brings about a northward moisture flux in association with northward wind anomalies in the lower troposphere over the Amur basin. This northward wind can then supply the Amur basin with moisture in association with the strengthened Asian summer monsoon. A west-to-east wavy pattern crossing the Eurasian continent at approximately 40° N, along the core of a climatological subtropical westerly jet, is clearly visible at 200-hPa height. This wave train is possibly a stationary Rossby wave that originated over western Europe. The cyclonic circulation around Lake Baikal, which directly influences the discharge, is thus related to this hemispheric midlatitude circulation.

[30] Winter atmospheric patterns associated with the winter flux of the stationary component have similar con-

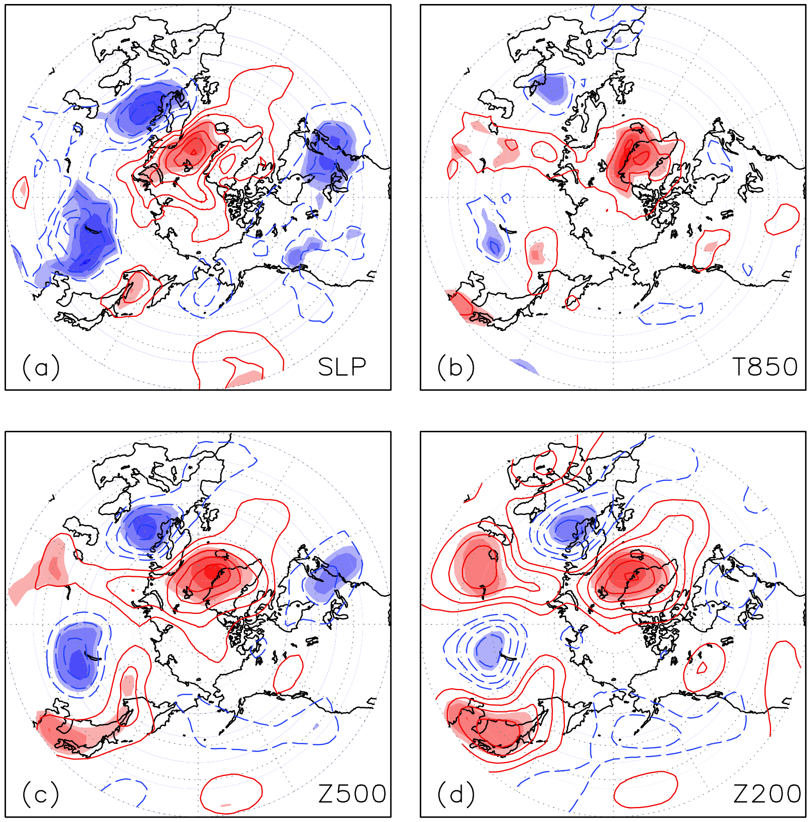

Figure 8. Linearly regressed summer (May, June, July, and August) mean large-scale patterns with the standardized interannual variation in the summer flux convergence of the stationary component. The data shown in this figure are from ERA40. (a) The sea level pressure, (b) the 850-hPa temperature, (c) the 500-hPa height, and (d) the 200-hPa height. Contour intervals for the height, SLP, and 850-hPa temperature are every 30 m, 0.2 hPa, and 0.2 K, respectively. The gradation of the shadings indicates statistical significance exceeding the 90, 95, 99, and 99.9% levels by the *t* test, assuming that the value in each year is independent. Warm and cool colors indicate positive and negative correlations, respectively.

tinent-to-ocean contrast in the SLP field to that in summer (Figure 9). Significant positive SLP anomalies widely cover the Okhotsk and Bering seas, signifying the weakness of the Aleutian low. Also, over Lake Baikal, significant negative anomalies appear in the SLP field. This feature implies the weakness of the winter Siberian high. Weakness of both the Siberian high and Aleutian low causes weakening of the Asian winter monsoon, which usually blows from the continent to the Pacific. This atmospheric pattern is consistent with the moisture flux pattern in winter (Figure 7). The weak winter monsoon wind over the Amur basin can suppress the evaporation there. For this reason, the moisture flux divergence over the basin in years of large winter P-E can be weaker than in years of small winter P-E.

[31] In addition, a hemispheric-scale pattern shows negative anomalies in the Arctic and positive anomalies in midlatitudes from the surface to the upper troposphere at 200-hPa height, although statistical significance is low in some areas. This northern low and southern high pattern and the temperature anomalies that are positive over the Eastern Hemisphere and negative over the Western Hemisphere are similar to the pattern of the positive phase of NAM/AO [e.g., *Thompson and Wallace*, 1998]. This indicates that the NAM/AO pattern tends to be positive in winter with the large moisture flux. The positive phase of the NAM/AO is related to the weakened eastern Asian winter monsoon [e.g., *Jhun and Lee*, 2004]. Therefore, the relation of this large moisture flux to the positive phase of NAM/AO is consistent with previous studies. However, the pattern in Figure 9c does not show a significant signature over the North Pacific Ocean, which usually has a significant signature in the typical NAM/AO pattern.

9. Discussion

[32] We have shown the relationship of Amur River discharge with atmospheric moisture flux from the perspective of interannual variation. *Ogi and Tachibana* [2006] demonstrated good correlation between the annual mean NAM/AO and the annual mean discharge. Our results for P-E over the Amur basin also show a NAM/AO-like signature in winter, but the NAM signature is not as clear as that found by *Ogi and Tachibana* [2006]. The correlation coefficient for the winter P-E with the spring discharge is smaller than that of the summer P-E with the autumn discharge (Figure 5). This small correlation implies that processes other than the winter P-E govern the spring discharge. Here, we suggest one possibility. Excluding the influence of the winter P-E from the spring discharge provides the interannual variation in spring discharge that is not explained by the

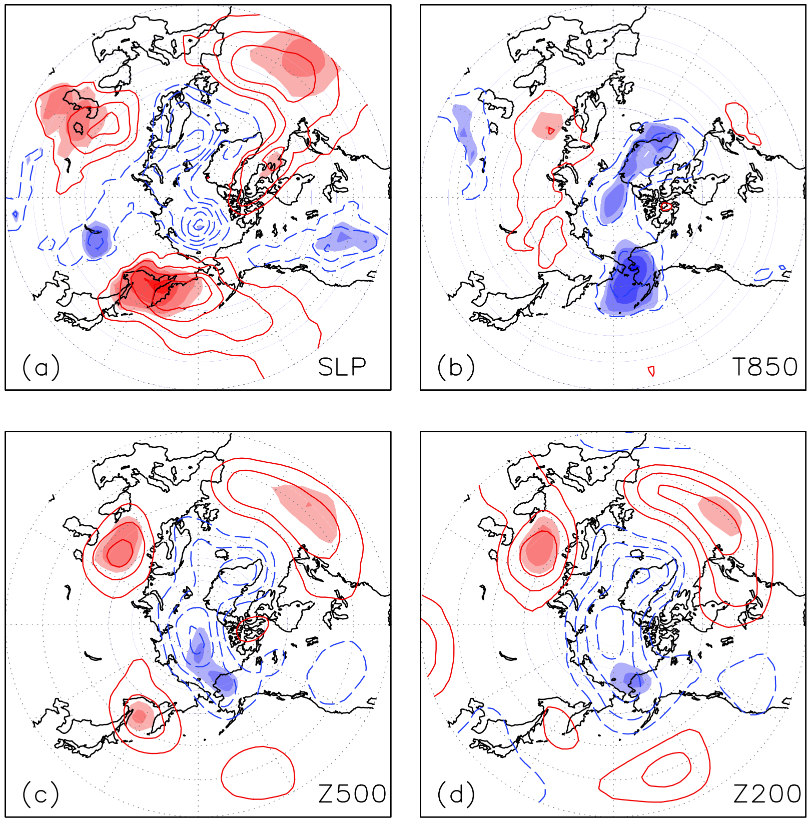

Figure 9. (a-d) As in Figure 8 except for winter (September to April) mean large-scale patterns with the standardized interannual variation in the winter flux convergence of the stationary component.

winter P-E or by the winter moisture flux. Subtracting the winter P-E from the spring discharge resulted in a value of $-\partial S/\partial t$ (equation (3)). Thus, the residual time series (R − P + E) corresponds to the interannual variation in discharge that is explained not by P-E, but by the change in storage, *S*.

[33] Figure 10 shows correlated and linearly regressed atmospheric patterns averaged for March, April, and May onto the standardized residual time series. The atmospheric pattern exhibited in Figure 10 can signify the large-scale pattern that is not related to the P-E, but is related to the change in *S*. The pattern has a significant signature of NAM/AO. The signature of the weak Aleutian low is particularly outstanding from the surface to the upper troposphere. In addition, the Amur basin is covered by significant warm anomalies in association with the weak Aleutian low. Thus, the residual spring discharge that is explained by the change in *S* is related to the warm anomalies with the NAM-related weak Aleutian low over the basin. Warmth can reduce *S* by promoting the melting of snow and frozen soil, both of which store water in its solid state. In fact, the climatological surface temperature in the Amur basin changes from negative to positive degrees Celsius in April as shown in Figure 2, implying that anomalous warm temperatures in April promote the melting of snow and frozen soil. It is therefore reasonable that the warmth associated with the NAM/AO was related to the large spring residual discharge. Solid state water only melts when the temperature is higher than the melting point, and the amount of meltwater is roughly related to the degrees of departure of the surrounding air temperature from the freezing point. We thus calculated an area-weighted average monthly mean air temperature at 2 m over the Amur basin using ERA40 data only when the monthly mean temperature of a grid point was higher than the melting point and calculated in April in each year. In a year when this value is large, a large amount of melting is expected. The correlation coefficient between this value and the residual time series on an interannual time scale is 0.50. Although the correlation is not high, it is positive. This positive correlation supports the idea that the warmth related to the spring NAM/AO promotes the melting and the discharge. To confirm this further, in our next study, we will use a regional hydrological model or other methods to examine hydrological thermodynamic processes.

10. Remarks

[34] Using long-term discharge data to analyze horizontal moisture flux, we have uncovered processes that determine Amur River discharge and their climatological seasonal and interannual variations. Comparison of the moisture flux to the discharge showed that the climatological spring discharge, which peaks in May, is supplied by the moisture flux in the previous autumn and winter. Table 4 summarizes the related atmospheric patterns. The autumn discharge peak is supplied by the summertime moisture flux. The spring discharge is mainly supplied by short-lived storm activity from the previous autumn and winter, whereas the

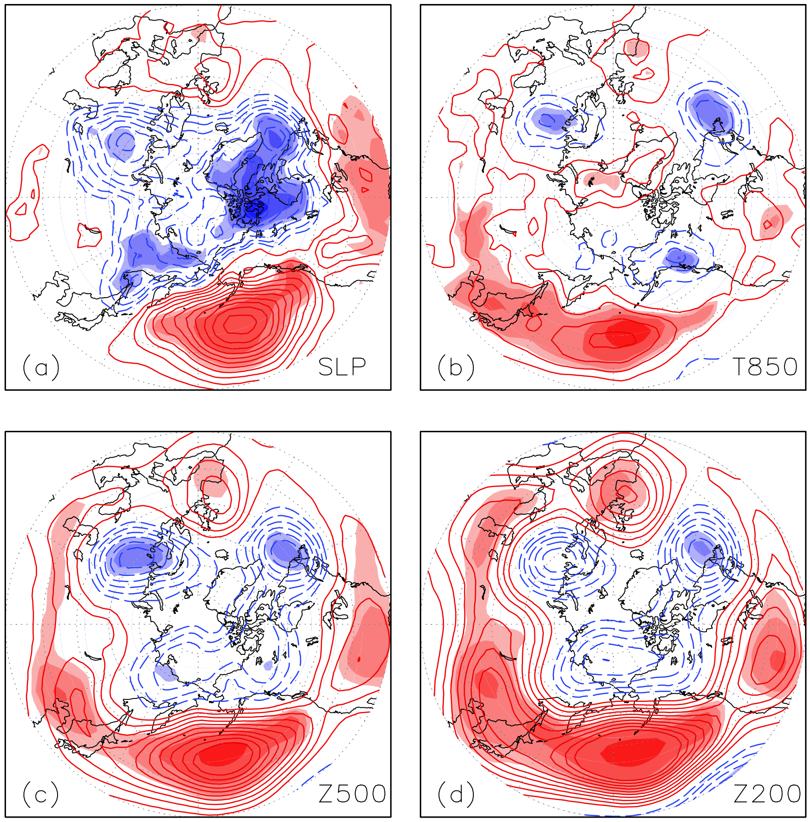

Figure 10. Linearly regressed atmospheric patterns averaged in March, April, and May onto the interannual time series of the change in land water storage, $-\partial S/\partial t$, which is calculated by a residual time series. The residual time series is the time series of the winter P-E subtracted from the spring discharge R. The time series of $-\partial S/\partial t$ is normalized. The plots illustrate typical atmospheric patterns in the years when spring storage shows an anomalously large decrease. The large decrease in storage partially contributes to the anomalously large spring discharge. Contours and shadings are the same as those in Figure 8.

autumn discharge is mainly supplied by stationary atmospheric patterns in association with the Asian summer monsoon and midlatitude westerlies.

[35] Interannual variation in the summer moisture flux is related to the strength of the Asian summer monsoon and a stationary anticyclone, the Okhotsk high. The Asian summer monsoon, in association with anomalous cyclonic circulation over Eurasia, strengthens the anomalously large summer moisture flux from the south, resulting in anomalously large discharge in autumn. The Asian winter monsoon, in association with the anomalously strong Siberian high and Aleutian low, strengthens the moisture flux divergence (i.e., activated evaporation in the Amur basin, resulting in anomalously small discharge in spring). The hemispheric atmospheric pattern relates to the moisture flux convergence and, to some extent, resembles the NAM/AO. Anomalously large spring discharge is also related to the warm phase of the NAM/AO, which prompts the melting of snow and frozen soil and thus contributes to the anomalously large spring discharge. Therefore, the NAM/AO pattern influences both the moisture flux and the change in land water storage.

[36] Finally, our results include oceanographic implications. Monsoon-related moisture flux to the Amur basin

Table 4. Summary of the Results[a]

	Autumn Discharge	Spring Discharge
Climatology	summer stationary moisture flux, from the south by the monsoon, from the inland by the westerlies	winter transient moisture flux, from the south by the storm track
Interannual	summer stationary moisture flux, strengthened summer monsoon	winter stationary moisture flux, weakened winter monsoon, AO-related spring warmth, melts of snow and frozen soil

[a]The "climatology" line indicates the large-scale atmospheric patterns corresponding to the climatological mean autumn and spring discharges. The "interannual" line indicates the related large-scale anomalous environments in a year of large discharge by the Amur River.

possibly originates from the subtropical Pacific Ocean. Thus, the following freshwater circulation is suggested. Moisture evaporated from the Pacific Ocean is brought to the Amur basin by the summer monsoon and then flows out to the Okhotsk Sea. Therefore, the Asian monsoon plays a role of northward freshwater transporter from the Pacific Ocean to the Okhotsk Sea. To confirm this, trajectory analysis or stable isotope observational studies are necessary to identify the source regions. Global warming might strengthen the Asian summer monsoon because of the enhancement of ocean-land temperature contrast. This strengthened monsoon may lead to reduced salinity in the Okhotsk Sea. The resulting freshening could then promote sea ice formation in the Okhotsk Sea in the future. In addition, the decrease in storage, S, in association with climate warming may also promote discharge and freshening. According to a multimodel ensemble analysis of the future large-river discharges due to global warming by *Nohara et al.* [2006], Amur River discharge will increase. Although *Nohara et al.* [2006] did not describe the reason for this increase, the influence of monsoon changes could be a possible cause. To confirm this, river discharge measurements at Bogorodskoe station must be maintained and continued into the future.

[37] **Acknowledgments.** The authors express their thanks to H. Hatsushika, K. Masuda, and M. J. Wallace for their invaluable suggestions. Comments by reviewers and an editor are also helpful for improvement of this paper. We deeply thank all the staff in Far Eastern Hydrometeorology and Environmental Monitoring, Russia, and all the staff in Far Eastern Regional Hydrometeorology Research Institute, Russia, in particular, M. A. Danchenkov and A. V. Gavarilov for their special effort to maintain the runoff observatory of Bogorodskoe. Without their effort, the measurement would have been stopped. This paper is a contribution to the Amur-Okhotsk Project (Human Activities in Northeastern Asia and Their Impact on the Biological Productivity in North Pacific Ocean), promoted by the Research Institute for Humanity and Nature, Japan. This project is an international collaborated research among Russia, China, and Japan. The Grid Analysis and Display System (GrADS) was used for drawing the figures.

References

Akagawa, M. (1977), Relation between flow of the Amur River and sea ice in the Okhotsk Sea (in Japanese), *J. Jpn. Soc. Snow Ice*, *39*, 1–6.

Alekseev, G. V., L. V. Bulatov, and V. F. Zakharov (2000), Fresh water freezing/melting cycle in the Arctic Ocean, in *The Fresh Water Budget of the Arctic Ocean*, edited by E. Lewis, pp. 589–608, Kluwer Acad., Boston, Mass.

Chen, S.-J., Y.-H. Kuo, P.-Z. Zhang, and Q.-F. Bai (1991), Synoptic climatology of cyclogenesis over east Asia, 1958–1987, *Mon. Weather Rev.*, *119*, 1407–1418, doi:10.1175/1520-0493(1991)119<1407:SCOCOE>2.0.CO;2.

Fukutomi, Y., H. Igarashi, K. Masuda, and T. Yasunari (2003), Interannual variability of summer water balance components in three major river basins of northern Eurasia, *J. Hydrometeorol.*, *3*, 249–266.

Gibson, J. K., P. Kållberg, S. Uppala, A. Nomura, A. Hernandez, and E. Serrano (1997), ERA description, *ECMWF ERA-15 Proj. Rep. Ser.*, *1*, Eur. Cent. for Med.-Range Weather Forecasts, Reading, U. K. (Available at http://www.ecmwf.int/publications)

Hirschi, M., S. I. Seneviratne, and C. Schar (2006), Seasonal variations in terrestrial water storage for major midlatitude river basins, *J. Hydrometeorol.*, *7*, 39–60, doi:10.1175/JHM480.1.

Inoue, T., and J. Matsumoto (2004), A comparison of summer sea level pressure over east Eurasia between NCEP-NCAR reanalysis and ERA-40 for the period 1960–99, *J. Meteorol. Soc. Jpn.*, *82*, 951–958, doi:10.2151/jmsj.2004.951.

Jhun, H., and E. Lee (2004), A east Asian winter monsoon index and associated characteristics of the winter monsoon, *J. Clim.*, *17*, 711–726, doi:10.1175/1520-0442(2004)017<0711:ANEAWM>2.0.CO;2.

Kanamitsu, M., W. Ebisuzaki, J. Woollen, S.-K. Yang, J. J. Hnilo, M. Fiorino, and G. L. Potter (2002), NCEP/DOE AMIP-II reanalysis (R-2), *Bull. Am. Meteorol. Soc.*, *83*, 1631–1643, doi:10.1175/BAMS-83-11-1631(2002)083<1631:NAR>2.3.CO;2.

Masuda, K., Y. Hashimoto, H. Matsuyama, and T. Oki (2001), Seasonal cycle of water storage in major river basins of the world, *Geophys. Res. Lett.*, *28*, 3215–3218, doi:10.1029/2000GL012444.

Murakami, T., and J. Matsumoto (1994), Summer monsoon over the Asian continent and western north Pacific, *J. Meteorol. Soc. Jpn.*, *72*, 719–745.

Nohara, D., A. Kitoh, M. Hosaka, and T. Oki (2006), Impact of climate change on river discharge projected by multimodel ensemble, *J. Hydrometeorol.*, *7*, 1076–1089, doi:10.1175/JHM531.1.

Numaguti, A. (1999), Origin and recycling processes of precipitating water over the Eurasian continent: Experiments using an atmospheric general circulation model, *J. Geophys. Res.*, *104*, 1957–1972, doi:10.1029/1998JD200026.

Ogi, M., and Y. Tachibana (2006), Influence of the annual Arctic Oscillation on the negative correlation between Okhotsk Sea ice and Amur River discharge, *Geophys. Res. Lett.*, *33*, L08709, doi:10.1029/2006GL025838.

Ogi, M., Y. Tachibana, F. Nishio, and M. A. Danchenkov (2001), Does the fresh water supply from the Amur river flowing into the Sea of Okhotsk affect sea ice formation?, *J. Meteorol. Soc. Jpn.*, *79*, 123–129, doi:10.2151/jmsj.79.123.

Oki, T., and Y. C. Sud (1998), Design of Total Runoff Integrating Pathway (TRIP)—A global river channel network, *Earth Interact.*, *2*(1), 1–36, doi:10.1175/1087-3562(1998)002<0001:DOTRIP>2.3.CO;2.

Oki, T., K. Musiake, H. Matsuyama, and K. Masuda (1995), Global atmospheric water balance and runoff from large river basins, *Hydrol. Processes*, *9*, 655–678, doi:10.1002/hyp.3360090513.

Onogi, K., et al. (2007), The JRA-25 reanalysis, *J. Meteorol. Soc. Jpn.*, *85*, 369–432, doi:10.2151/jmsj.85.369.

Oshima, K., and K. Yamazaki (2004), Seasonal variation of moisture transport in the polar regions and the relation with annular modes, *Polar Meteorol. Glaciol.*, *18*, 30–53.

Oshima, K., and K. Yamazaki (2006), Difference in seasonal variation of net precipitation between the Arctic and Antarctic regions, *Geophys. Res. Lett.*, *33*, L18501, doi:10.1029/2006GL027389.

Robinson, D. A., K. F. Dewey, and R. R. Heim Jr. (1993), Global snow cover monitoring: An update, *Bull. Am. Meteorol. Soc.*, *74*, 1689–1696, doi:10.1175/1520-0477(1993)074<1689:GSCMAU>2.0.CO;2.

Serreze, M. C., D. H. Bromwich, M. P. Clark, A. J. Etringer, T. Zhang, and R. Lammers (2002), Large-scale hydro-climatology of the terrestrial Arctic drainage system, *J. Geophys. Res.*, *107*, 8160, doi:10.1029/2001JD000919. [printed *108*(D2), 2003]

Su, F., J. C. Adam, K. E. Trenberth, and D. P. Lettenmaier (2006), Evaluation of surface water fluxes of the pan-Arctic land region with a land surface model and ERA-40 reanalysis, *J. Geophys. Res.*, *111*, D05110, doi:10.1029/2005JD006387.

Tachibana, Y., T. Iwamoto, M. Ogi, and Y. Watanabe (2004), Abnormal meridional temperature gradient and its relation to the Okhotsk high, *J. Meteorol. Soc. Jpn.*, *82*, 1399–1415.

Thompson, D. W. J., and J. M. Wallace (1998), The Arctic Oscillation signature in the wintertime geopotential height and temperature fields, *Geophys. Res. Lett.*, *25*, 1297–1300, doi:10.1029/98GL00950.

Uppala, S. M., et al. (2005), The ERA-40 reanalysis, *Q. J. R. Meteorol. Soc.*, *131*, 2961–3012, doi:10.1256/QJ.04.176.

Xie, P., A. Yatagai, M. Chen, T. Hayasaka, Y. Fukushima, C. Liu, and S. Yang (2007), A gauge-based analysis of daily precipitation over east Asia, *J. Hydrometeorol.*, *8*, 607–627, doi:10.1175/JHM583.1.

Yasuda, I. (1997), The origin of the North Pacific Intermediate Water, *J. Geophys. Res.*, *102*, 893–909, doi:10.1029/96JC02938.

Yoshino, M. (1965), Four stages of the rainy season in early summer over east Asia (part I), *J. Meteorol. Soc. Jpn.*, *43*, 231–245.

M. Ogi, Joint Institute for the Study of the Atmosphere and Ocean, University of Washington, Seattle, WA 98195, USA. (masayo@atmos.washington.edu)

K. Oshima, Faculty of Environmental Earth Science, Hokkaido University, Sapporo 060-0810, Japan. (kaz@ees.hokudai.ac.jp)

Y. Tachibana, Institute of Observational Research for Global Change, Japan Agency for Marine-Earth Science and Technology, Yokosuka 237-0061, Japan. (tachi@jamstec.go.jp)